Published in final edited form as:
Invest Radiol. 2014 October ; 49(10): 640–646. doi:10.1097/RLI.0000000000000066.

Assessment of Renal Artery Stenosis Using Intravoxel Incoherent Motion Diffusion-weighted MRI Analysis

Behzad Ebrahimi, Ph.D., **Naveen Rihal**, **John R. Woollard, M.Sc.**, **James D. Krier, M.Sc.**, **Alfonso Eirin, M.D.**, and **Lilach O. Lerman, M.D., PH.D**
Division of Nephrology and Hypertension, Mayo Clinic, Rochester, Minnesota.

Abstract

Objectives—Diffusion weighted MRI is a powerful tool to assess renal morphology. However, its quantitative index, apparent diffusion constant (ADC) derived from a conventional mono-exponential model can vary with both functional and structural alterations, as well as the choice of b-values. In contrast, the intravoxel incoherent motion (IVIM) bi-exponential model provides independent parameters that may represent broader aspects of renal pathophysiology. We hypothesize that IVIM analysis is capable of detecting early morphological and functional changes in the swine kidney distal to renal artery stenosis (RAS).

Materials and Methods—Domestic pigs divided into three groups (n=6–7 each) were studied for 16 weeks. Unilateral RAS was induced in two groups, of which one was fed with a high cholesterol diet to induce early atherosclerosis (ARAS), while the other (RAS) consumed regular diet. The third group included normal pigs which served as control sham. Renal function, hemodynamics, tubular function and morphology were assessed using multi-detector computed tomography (MDCT) and histology. Diffusion-weighted MR images were acquired at 3T and analyzed using mono and bi-exponential models. ADC and IVIM parameters (Diffusivity (D_t), flow-dependent pseudo-diffusivity (D_p), and fluid fraction (f_p)) were calculated in cortex and medulla of the stenotic (STK) and contra-lateral kidneys (CLK). Results were analyzed using ANOVA, student t-test, and regression analysis.

Results—In both RAS and ARAS the STK shrank and the CLK underwent hypertrophy. GFR and renal blood flow declined in STKs, and CLKs manifested hyperfiltration. Additionally, ARAS kidneys showed reduced mean transit time in distal tubular segments. ADC and diffusivity both decreased in STK of RAS and ARAS. D_p and f_p were elevated in both the STK and CLK of RAS and more prominently in ARAS. STK cortical ADC and D_t correlated inversely with the degree of fibrosis, and directly with GFR. Furthermore, D_p correlated with tubular injury score in all kidneys.

Conclusions—ADC and D_t both correlated with cortical and medullary fibrosis, however, IVIM-derived parameters can detect subtle functional and structural changes in the post-stenotic kidney, and may also serve as markers for tubular injury.

Corresponding author: Lilach Lerman, MD, Ph.D, Division of Nephrology and Hypertension, Mayo Clinic, 200 First St SW, Rochester, MN 55905. lerman.lilach@mayo.edu, Phone: (507) 266-9376, Fax: (507) 266-9316.

Keywords

Renal Artery Stenosis; Diffusion-weighted imaging; intravoxel incoherent motion

Introduction

Renal artery stenosis (RAS) is a vascular disorder, which may result in chronic kidney disease (CKD) and lead to end stage renal failure[1]. Significant RAS compromises renal blood flow (RBF), induces renovascular hypertension, impairs glomerular filtration rate (GFR), and induces interstitial fibrosis in the post-stenotic kidney (STK). While in the Western world atherosclerotic RAS (ARAS) is the predominant etiology in adults, RAS may be caused by other causes like fibromuscular dysplasia[1]. Renal injury in ARAS is more severe because atherogenic factors exacerbate damage in both the STK and the contralateral kidney (CLK)[2,3]. Early diagnosis and effective treatment may potentially slow further deterioration of renal function. Different imaging techniques and modalities have been used to detect and investigate mechanisms of renal functional and hemodynamic deterioration, yet assessment of tissue injury and morphological changes in the kidney is difficult without invasive methods[4–7].

Diffusion weighted imaging (DWI) MRI is a powerful technique, which is sensitive to changes in microstructure of biological tissues[8]. Independence from exogenous contrast agents makes DWI particularly attractive for kidney injury assessment in patients with compromised kidney function, who are at increased risk of nephrogenic systemic fibrosis following gadolinium-enhanced imaging[9]. Apparent diffusion coefficient (ADC), a quantitative index of DWI, can be calculated by fitting the MR signal intensity obtained from images with different diffusion-weighting to a mono-exponential decay model. This approach has been used for the analysis of a broad range of renal pathological conditions, likely because of its simplicity and the feasibility of implementation with as few as two sets of diffusion-weighed images. A decrease in ADC has often been attributed to structural changes such as interstitial fibrosis or tubular atrophy, and demonstrated to correlate with renal function[10–13]. Nevertheless, flow-dependency of ADC complicates results interpretation, particularly within the STK in which structural and hemodynamic alterations coexist[14].

Le Bihan et. al. showed that pure diffusion and perfusion-dependent diffusion can be separated using the intra-voxel incoherent motion (IVIM) analytical technique, which applies a bi-exponential model to MR signal intensity decay[15]. This model is based on the premise that the decay of MR intensity in biological tissues results from both a flow-dependent fast signal decay (pseudo-diffusion), and a flow-independent slow decay, determined by pure diffusion in tissue structures (diffusivity). Therefore, in addition to crude kidney morphology, IVIM affords information about microvascular and tubular fluid dynamics, which makes it particularly appealing for studying the STK. However, application of IVIM in the STK has not been fully evaluated partly due to technical limitations of MRI in previous years[16,17]. In the past few years, robust hardware and improved sequences for body-DWI have encouraged re-examination of this analytical

method in the kidney[18]. Recent studies demonstrated the capability of IVIM in reducing b-value dependency of diffusivity, the response of IVIM parameters to pharmacological challenges[19], and providing biomarkers for different pathological conditions, such as renal tumors[20]. However, the feasibility of illustration of renal functional and structural alterations in RAS using IVIM has not been fully examined.

We hypothesize that functional and morphological alterations in the swine STK and CLK, illustrated by multi-detector computed tomography (MDCT) and histology, would be accompanied by corresponding changes in DWI-derived diffusivity and pseudo-diffusivity calculated using the IVIM model. We further hypothesize that DWI-derived parameters would depict greater renal impairment in pigs with ARAS compared to RAS.

Materials and Methods

All animal procedures followed the Guideline for the Care and Use of Laboratory Animals (National Research Council, National Academy Press, Washington, DC, 1996) and were approved by the Institutional Animal Care and Use Committee.

Nineteen female domestic pigs were studied for 16 weeks. Six of the animals were fed a high cholesterol diet for the entire course of the study to induce early atherosclerosis, starting six weeks before and continued until ten weeks after the induction of stenosis. The remaining thirteen animals were fed with a regular diet. One group (n=6) underwent a sham procedure (Sham) while unilateral RAS was induced in seven of the pigs fed normal chow (n=7 RAS) and in the entire high-cholesterol diet group (n=6) (ARAS), by placing an irritant coil in the right main renal artery[21].

DWI scans were performed 10 weeks after RAS or Sham, and renal volume and hemodynamics assessed using MDCT, 2–3 days later. Prior to each in vivo study animals were anesthetized with 0.25g of intramuscular tiletamine hydrochloride/zolazepam hydrochloride and 0.5g of xylazine, and anesthesia maintained with intravenous ketamine (0.2mg/kg/min) and xylazine (0.03mg/kg/min) (for CT), or inhaled 1–2% isoflurane (for MRI) throughout the course of imaging. The degree of stenosis was assessed by renal angiography[22], blood samples collected from a central venous catheter during CT studies, and mean arterial pressure (MAP) measured using an arterial catheter.

Animals were eventually euthanized with a lethal intravenous dose of sodium pentobarbital (100mg/kg, Fatal Plus, Sleepaway, Fort Dodge Laboratories, Fort Dodge, Iowa) a few days after completion of in vivo studies. Then the kidneys were removed, dissected and stored at −80°C or preserved in formalin for histology.

DWI was performed on a 3T scanner (GE Medical Systems, Milwaukee, Wisconsin) using a torso array coil. Images were collected using a single-shot echo-planar sequence with bipolar gradients. Four to Six coronal slices in oblique planes were collected during suspended respiration for b-values 0, 50, 100, 200, 300, 600, 800 and 1000 s/mm^2. MR parameters were set to TR/TE 1800/79ms, field of view 35cm, Bandwidth 648Hz/pixel, number of averages 3, slice thickness 2.5mm, and matrix size 128×128.

MDCT imaging

We have previously shown that MDCT-derived assessments of renal size and function agree well with reference standards[4]. Contrast media were injected during scanning through a pigtail catheter, advanced through the left jugular vein to the superior vena cava. Following catheterization, the animals were moved to MDCT unit (Somatom Sensation 64; Siemens Medical Solutions, Forchheim, Germany). Initial tomographic positioning was determined with pilot scans. A bolus of iopamidol (0.5 ml/kg over 2s) was then injected, and 140 consecutive scans acquired 3 seconds later, over approximately 3 minutes, as previously shown[4].

Following the flow scan a volume study was performed after an additional contrast injection. Axial images were acquired in the helical mode with thickness of 0.6mm and resolution of 512×512, and reconstructed at 5mm thickness. Kidney volumes were calculated using planimetry from contrast-enhanced vascular phase images.

Morphological Studies

Renal fibrosis and tubular injury score were quantified from 5μm thick axial sections stained for trichrome and Hematoxylin and eosin. For each kidney 10–15 images were acquired at 20× (fibrosis) or 40× (tubular injury score) using a microscope (ZEN® 2012 blue edition Carl ZEISS SMT, Oberkochen, Germany). The fraction of fibrotic tissue in each cortex and medulla was estimated semi-automatically, using a colorimetric approach. Tubular injury score was determined according to the area of kidney (1, <25%; 2, 25%≤ <50%; 3, 50%≤ <75%; 4, 75%≤ <100%) affected by tubular luminal obstruction, cell detachment, and intratubular cast formation[23].

Data Analysis

All MR and MDCT analyses were performed (by B.E., 4 years of experience and J.D.K., 17 years of experience, respectively) in MATLAB® (MathWork, Natick, MA, USA) and Analyze™ (Biomedical Imaging Resource, Mayo Clinic, MN, USA).

IVIM—IVIM, bi-exponential model[14]:

$$S=S_0((1-f_p).e^{-bD_t}+f_p.e^{-b(D_p+D_t)}) \quad (1)$$

was used to calculate the tissue fluid fraction (f_p), which reflects tissue dynamic fluid content, pseudo-diffusivity (D_p) that is sensitive to flow velocity within renal vessels and tubules, and diffusivity (D_t) that reflects water molecules free diffusion, and is sensitive to microstructural barriers which may limit free diffusion. S_0 is the MR signal intensity in DWI images for b=0 (b_0). The assumption underlying IVIM is that in Equation (1) the first term is sensitive to pure diffusivity, whereas the second term mainly reflects flow-weighted phenomena. D_t and f_p were estimated from the segment of the curve corresponding to b-values > 200 s/mm^2, and in the second step, D_p was estimated from the entire curve. Pixel-by-pixel maps were generated for all the IVIM parameters for each slice (Figure 1). Inter-observer agreement was assessed by calculating the intra-class correlation coefficients (ICC)

along with 95% confidence intervals (CI) for all IVIM parameters in cortex and medulla (B.E. and N.R., 3 months of experience).

ADC—ADC maps were generated for the cortex and medulla by pixel-by-pixel fitting the curve of MR signal intensity vs. corresponding b-values to a mono-exponential decay model.

Regions of interest (ROIs) were drawn on the b_0 DWI images and transferred to the maps. In the cortex, maps were sampled using single large ROI, whereas in the medulla, ROIs were determined by the size and the number of visible medullary tissue segments (Figure 1). Cortical and medullary mean values for ADC and each IVIM parameter for each animal were calculated by averaging values from all corresponding sampled ROIs.

MDCT—Using contrast-enhanced MDCT, cortical and medullary volumes, regional renal perfusion, vascular and tubular mean transit times (MTT), fractional blood volume (FBV), GFR and RBF were calculated. The volumes of the cortex and medulla were determined from the total tomographic areas of each compartment multiplied by the 5mm thickness of cross-sectional images. To calculate renal function and hemodynamics, the cortical and medullary signal attenuation vs. time curves were fitted to an extended Γ-variate model. This model yields curve-fitting parameters that allow calculation of regional FBV and vascular and tubular MTTs, in the proximal tubule, Henle's loop, and distal tubule, as previously reported[24]. These parameters were in turn used to calculate cortical and medullary perfusion and blood flows (products of the perfusion and corresponding volumes). Total RBF was assessed as the sum of cortical and medullary flow. Finally, single-kidney regional GFR was evaluated using the cortical curve and the slope of the proximal tubular curves, as previously shown[24]. Total kidney GFR was calculated by multiplying the regional GFR and the cortical volume.

Statistical Analysis

Results are presented as mean±SEM. ANOVA was used for STK/CLK comparison and among groups, followed by unpaired t-test. Regression analysis was performed using the least square method, in some cases on a compiled set of corresponding kidneys from all three groups of RAS, ARAS and Sham. For p values ≤ 0.05, results were considered significant.

Results

Ten weeks after RAS induction the degree of stenosis in the RAS and ARAS groups were comparable and MAP was similarly elevated (Table. 1). The cortical and medullary regions of the STKs underwent atrophy and a decrease in RBF, whereas in the CLKs, the cortex showed hypertrophy, and medullary volumes remained unchanged. MDCT-derived GFR was reduced in the STKs and elevated in the CLKs compared to the sham group. Cortical vascular and proximal tubular MTT values were similar among all groups, whereas distal MTT was significantly shorter in the ARAS STK and CLK, and tended to be shorter in RAS as well (p=0.063 and p=0.072 in the STK and CLK, respectively). Cortical perfusion and FBV remained unchanged, while medullary perfusion and FBV declined in all STKs.

Tissue Morphology

The degree of fibrosis was significantly higher in the cortex and medulla of both the STK and CLK of ARAS compared to those in RAS or shams, suggesting greater tissue injury in ARAS. Interstitial fibrosis (trichrome-staining) in the cortex of RAS STK was also greater than Sham (Figure 2.A–B). Medullary fibrosis was elevated compared to sham in all RAS and ARAS kidneys, but again in ARAS more than in RAS. Tubular injury score was significantly higher in the RAS STK and in both ARAS kidneys compared to Sham (Figure 2.C–D).

IVIM parameters

RAS STK cortical diffusivity was significantly lower than that in its CLK or in sham, while the RAS CLK and Sham were similar. In contrast, ARAS STK diffusivity was not different than its CLK, yet was reduced compared to the Sham, and tended to decrease in the CLK as well (p= 0.084 vs. sham) (Figure 3). Similarly, in RAS f_p was higher than Sham in the STK and tended to be elevated in the CLK (p=0.060), whereas in ARAS, both were significantly higher compared to sham Control. Finally, cortical pseudo-diffusivity (flow velocity) was elevated in STK and CLK of both RAS and ARAS, except that in the RAS STK the increase has not reached statistical significance (p=0.067).

A similar pattern was observed in the medulla, where diffusivity tended to decline in the RAS STK (p=0.091) and in both ARAS STK and CLK (p=0.072 and p=0.095 in RAS and ARAS, respectively and p=0.020 in RAS CLK vs. ARAS CLK) while pseudo-diffusivity was significantly elevated in all STKs and CLKs, except in RAS STK (p=0.058 vs. Sham). f_p was only increased in both ARAS but not RAS kidneys.

Inter-observer agreement ICC for D_t, F_p and D_p were 0.95 (CI: [0.84–0.98]), 0.95 (CI: [0.83–0.98]) and 0.93 (CI: [0.76–0.98]) in cortex and 0.90 (CI: [0.67–0.97]), 0.91 (CI: [0.70–0.97]), and 0.88 (CI: [0.63–0.97]) in medulla.

ADC

In both the cortex and medulla, ADC values were significantly lower in the STK compared to the CLK and Sham, whereas CLK ADC were not different than Sham (Figure 3.d & 3.h).

Analysis of Regression

Cortical and medullary diffusivity and ADC showed strong correlation in all kidneys (Figure 4). In the STK, cortical and medullary diffusivity and ADC, all correlated inversely with the histological degree of fibrosis and in the cortex also with GFR (Figure 5.A–B). Pseudo-diffusion in the cortex of all kidneys correlated inversely with MDCT-derived distal tubular MTT (Figure 5.C). Furthermore, STK (but not CLK) cortical f_p showed a modest but significant correlation with MDCT-derived FBV, and inversely correlated with the degree of fibrosis. Tubular injury score correlated with cortical pseudo-diffusivity (Figure 5.D).

Discussion

This study shows that IVIM-based analysis of DWI can detect and distinguish functional and morphological changes in atherosclerotic (ARAS) and non-atherosclerotic RAS kidneys, which agree with comparable assessments, obtained using independent methods. Diffusivity decreased in the STKs and inversely correlated to the histological degree of fibrosis. Fluid fraction and pseudo-diffusivity increased in the RAS STK cortex, and remarkably in both ARAS STK and CLK, suggesting tubular functional and structural alterations, as confirmed by MDCT and histology. Therefore, this study suggests that DWI parameters may serve as biomarkers of kidney injury.

The results of this study indicated that IVIM is capable of unraveling renal morphological and fluid dynamic alterations in RAS and ARAS subjects. Ten weeks after induction of stenosis, we observed hallmarks of RAS, including a decline in STK volume RBF, and GFR, and development of systemic hypertension. Because of the relatively moderate degree of stenosis, the main changes were related to renal volume, so that STK atrophy and compensatory CLK hypertrophy largely preserved regional GFR, FBV, and perfusion[25]. Nevertheless, cortical diffusivity fell in both RAS and ARAS STK and tended to decrease in their medulla as well. Indeed, diffusivity correlated with the level of fibrosis, which was elevated in the RAS STK and in both ARAS kidneys. Smaller diffusivity of ARAS vs. RAS medullary CLK (which was not different than the ARAS STK) was likely attributed to greater fibrosis and structural alterations found in ARAS CLK by histology. Notably, this was consistent with our previous finding that the morphology of the RAS CLK remains largely preserved, whereas in ARAS the additive systemic effects of atherosclerosis and hypertension adversely impact CLK tissue[2,3]. Cortical diffusivity also correlated with GFR in the STK. Lack of such correlation in the CLK is particularly interesting, considering that CLK GFR was significantly increased to compensate for the reduced STK GFR. This may imply that the increase in CLK GFR is driven mostly by renal functional rather than structural changes, whereas in the STK, both morphological (e.g. fibrosis, glomerulosclerosis) and hemodynamic factors contribute to the diminished GFR.

In addition to diffusivity, which is often attributed to morphological changes in the tissue[26,27], IVIM analysis yields D_p and f_p. D_p has been shown to be sensitive to both vascular blood and tubular fluid velocities[17,28], while f_p is the ratio of vascular and tubular fluid volume to the total fluid in the tissue[19]. Our study suggests that cortical and medullary fluid velocities increased in both ARAS kidneys and in RAS CLK, and tended to rise in the RAS STK. The use of MDCT allowed attributing the increased D_p to tubular flow velocity. Notably, in our model with moderate stenosis and sustained STK perfusion, MDCT showed that vascular MTT remained unchanged, whereas in ARAS kidneys shorter distal tubular MTT implied higher flow velocity in this tubular segment in ARAS kidneys. Remarkably, DWI MRI-derived D_p correlated significantly and inversely with distal tubular MTT, but not with vascular MTT, suggesting that in this study, increases in D_p reflects primarily faster tubular flow variations. In support of this stipulation, D_p also directly correlated with the histological tubular injury score, which established tubular morphological alterations. Some tubular injuries such as cell detachment and intratubular cast formation may affect tubular fluid dynamic by increasing tubular resistance and fluid velocity, yet reducing overall

tubular flow and urine volume[29]. Moreover, this speculation is concordant with findings in ischemic tubular injury which shows collecting ducts and particularly distal tubules are the primary cites of obstruction by tubular debris, cells and polymerized Tamm-Horsfall protein[30]. On the other hand, the increase in f_p might have resulted from extracellular matrix accumulation in the atrophic STK[2] that decreases interstitial fluid to a greater extent than tubular fluid volume. This is suggested by the inverse correlation of STK cortical fibrosis and f_p.

Higher f_p and D_p in the CLK, which is subjected to increased filtration and pressure natriuresis, are concordant with purported increases in healthy subjects during diuresis[19], as a result of elevated GFR and tubular flow. In our study, CLK hyperfiltration due to the increased arterial pressure also serves as a compensatory mechanism that increases CLK GFR but not the number of nephrons. Hence, an increase in f_p may reflect an increase in tubular flow in response to the CLK fluid overload. These observations suggest that an increase of f_p alone may not distinguish functional from structural underlying causes.

The mono-exponential model provided results that were in close agreement to a previous study in RAS[10], and demonstrated decreased renal ADC that correlated with renal function and the degree of fibrosis. Moreover, good correlation between the diffusivity and ADC values, as well as their correlations with the degree of fibrosis and GFR, highlighted the similarity of these two indices. Although ADC was influenced by low b-values, as suggested by higher values of ADC compared to diffusivity, its characteristics were predominantly determined by the high b-values.

Therefore, this study demonstrates that IVIM analysis affords information beyond that provided by ADC, and allows detecting discernible renal alterations in RAS and ARAS. Diffusivity was linked to morphological changes, which were likely driven mainly by fibrosis. D_p might depend on tubular injury in the STK, and on increased tubular flow in the CLK. Similarly, f_p was sensitive to morphological changes in the STK and functional alterations in the CLK. Although currently incapable of differentiating the contribution of the vascular from tubular sub-compartments to f_p and D_p, our study implies that IVIM can provide useful markers of renal tubular function. Conceivably a combination of arterial spin labeling and DWI scans may help distinguish these two functional aspects, based on different times-of-flight, and thereby facilitate their interpretation and provide more specific markers for tubular function and hemodynamics. Notably, we also found that morphological and functional alterations in the STK alone could be adequately depicted using ADC. Yet as previous studies have shown, b-value-dependency and inconsistent selection of b-values have complicated derivation of reliable and reproducible values of ADC[14]. Furthermore, the mono-exponential model cannot differentiate the contribution of functional from morphological alterations or distinguish subtle differences in injury severity (ARAS from RAS). Nevertheless, the relative simplicity of use may make analysis of ADC attractive for assessment of renal injury, when considerable in extent.

This study had some limitations. Animals used in this study were relatively young, and we cannot rule out an influence of age-related factors. Furthermore, due to intrinsic distortion in EPI[31], co-registration of diffusion images with those with enhanced corticomedullary

differentiation was difficult, and medullary ROIs were drawn on b_0 images, which might have introduced some error to our data analysis. Medullary analysis is also more prone to error due to its smaller size. Large variations in the Sham medullary data prevented achievement of statistical significance in some measurements. Additionally, our hemodynamic and the DWI data were collected on different imaging sessions, which may have also introduced some small physiological variations.

In conclusion, this study shows that IVIM parameters are sensitive to fibrosis (e.g. mild degree of fibrosis in the CLK) and alterations in tubular flow as a result of functional or structural tubular alterations in unilateral RAS and ARAS. DWI is a powerful method to assess selective pathological markers in the kidney. Independence from exogenous contrast-agents makes this imaging technique appealing to use for patients with chronic kidney disease. Further studies are needed to determine the utility of these techniques in patients with ARAS.

Acknowledgments

This study was partly supported by National Institutes of Health Grants Numbers HL77131, DK73608, C06RR018898, and HL121561 and by a postdoctoral fellowship (B.E.) from the Mayo Clinic Center for Regenerative Medicine.

References

1. Safian RD, Textor SC. Renal-artery stenosis. N Engl J Med. 2001 Feb 8; 344(6):431–442. [PubMed: 11172181]
2. Chade AR, Rodriguez-Porcel M, Grande JP, et al. Mechanisms of renal structural alterations in combined hypercholesterolemia and renal artery stenosis. Arterioscler Thromb Vasc Biol. 2003 Jul 1; 23(7):1295–1301. [PubMed: 12750121]
3. Urbieta-Caceres VH, Lavi R, Zhu XY, et al. Early atherosclerosis aggravates the effect of renal artery stenosis on the swine kidney. Am J Physiol Renal Physiol. 2010 Jul; 299(1):F135–F140. [PubMed: 20462971]
4. Daghini E, Primak AN, Chade AR, et al. Assessment of renal hemodynamics and function in pigs with 64-section multidetector CT: comparison with electron-beam CT. Radiology. 2007 May; 243(2):405–412. [PubMed: 17456868]
5. Avasthi PS, Voyles WF, Greene ER. Noninvasive diagnosis of renal artery stenosis by echo-Doppler velocimetry. Kidney Int. 1984 May; 25(5):824–829. [PubMed: 6236324]
6. Schoenberg SO, Knopp MV, Bock M, et al. Renal artery stenosis: grading of hemodynamic changes with cine phase-contrast MR blood flow measurements. Radiology. 1997 Apr; 203(1):45–53. [PubMed: 9122415]
7. Prince MR, Schoenberg SO, Ward JS, et al. Hemodynamically significant atherosclerotic renal artery stenosis: MR angiographic features. Radiology. 1997 Oct; 205(1):128–136. [PubMed: 9314974]
8. Hueper K, Rong S, Gutberlet M, et al. T2 relaxation time and apparent diffusion coefficient for noninvasive assessment of renal pathology after acute kidney injury in mice: comparison with histopathology. Invest Radiol. 2013 Dec; 48(12):834–842. [PubMed: 23907103]
9. Perazella MA, Rodby RA. Gadolinium-induced nephrogenic systemic fibrosis in patients with kidney disease. Am J Med. 2007 Jul; 120(7):561–562. [PubMed: 17602923]
10. Yildirim E, Kirbas I, Teksam M, et al. Diffusion-weighted MR imaging of kidneys in renal artery stenosis. Eur J Radiol. 2008 Jan; 65(1):148–153. [PubMed: 17537606]
11. Yang D, Ye Q, Williams DS, et al. Normal and transplanted rat kidneys: diffusion MR imaging at 7 T. Radiology. 2004 Jun; 231(3):702–709. [PubMed: 15163810]

12. Xu Y, Wang X, Jiang X. Relationship between the renal apparent diffusion coefficient and glomerular filtration rate: Preliminary experience. Journal of Magnetic Resonance Imaging. 2007; 26(3):678–681. [PubMed: 17729335]
13. Togao O, Doi S, Kuro-o M, Masaki T, Yorioka N, Takahashi M. Assessment of renal fibrosis with diffusion-weighted MR imaging: study with murine model of unilateral ureteral obstruction. Radiology. 2010 Jun; 255(3):772–780. [PubMed: 20406881]
14. Zhang JL, Sigmund EE, Chandarana H, et al. Variability of renal apparent diffusion coefficients: limitations of the monoexponential model for diffusion quantification. Radiology. 2010 Mar; 254(3):783–792. [PubMed: 20089719]
15. Le Bihan D, Breton E, Lallemand D, et al. Separation of diffusion and perfusion in intravoxel incoherent motion MR imaging. Radiology. 1988 Aug; 168(2):497–505. [PubMed: 3393671]
16. Powers TA, Lorenz CH, Holburn GE, et al. Renal artery stenosis: in vivo perfusion MR imaging. Radiology. 1991 Feb; 178(2):543–548. [PubMed: 1987621]
17. Koh DM, Collins DJ, Orton MR. Intravoxel incoherent motion in body diffusion-weighted MRI: reality and challenges. AJR Am J Roentgenol. 2011 Jun; 196(6):1351–1361. [PubMed: 21606299]
18. Heusch P, Wittsack HJ, Heusner T, et al. Correlation of biexponential diffusion parameters with arterial spin-labeling perfusion MRI: results in transplanted kidneys. Invest Radiol. 2013 Mar; 48(3):140–144. [PubMed: 23249648]
19. Sigmund EE, Vivier PH, Sui D, et al. Intravoxel incoherent motion and diffusion-tensor imaging in renal tissue under hydration and furosemide flow challenges. Radiology. 2012 Jun; 263(3):758–769. [PubMed: 22523327]
20. Chandarana H, Lee VS, Hecht E, et al. Comparison of biexponential and monoexponential model of diffusion weighted imaging in evaluation of renal lesions: preliminary experience. Invest Radiol. 2011 May; 46(5):285–291. [PubMed: 21102345]
21. Lerman LO, Schwartz RS, Grande JP, et al. Noninvasive evaluation of a novel swine model of renal artery stenosis. J Am Soc Nephrol. 1999 Jul; 10(7):1455–1465. [PubMed: 10405201]
22. Chade AR, Rodriguez-Porcel M, Grande JP, et al. Distinct renal injury in early atherosclerosis and renovascular disease. Circulation. 2002 Aug 27; 106(9):1165–1171. [PubMed: 12196346]
23. Ebrahimi B, Eirin A, Li Z, et al. Mesenchymal stem cells improve medullary inflammation and fibrosis after revascularization of swine atherosclerotic renal artery stenosis. Plos One. 2013; 8(7):e67474. [PubMed: 23844014]
24. Krier JD, Ritman EL, Bajzer Z, et al. Noninvasive measurement of concurrent single-kidney perfusion, glomerular filtration, and tubular function. Am J Physiol Renal Physiol. 2001 Oct; 281(4):F630–F638. [PubMed: 11553509]
25. Schoenberg SO, Aumann S, Just A, et al. Quantification of renal perfusion abnormalities using an intravascular contrast agent (Part 2): Results in animals and humans with renal artery stenosis. Magnet Reson Med. 2003 Feb; 49(2):288–298.
26. Chandarana H, Kang SK, Wong S, et al. Diffusion-weighted intravoxel incoherent motion imaging of renal tumors with histopathologic correlation. Invest Radiol. 2012 Dec; 47(12):688–696. [PubMed: 22996315]
27. Thoeny HC, De Keyzer F, Oyen RH, et al. Diffusion-weighted MR imaging of kidneys in healthy volunteers and patients with parenchymal diseases: Initial experience. Radiology. 2005 Jun; 235(3):911–917. [PubMed: 15845792]
28. Muller MF, Prasad PV, Edelman RR. Can the IVIM model be used for renal perfusion imaging? European Journal of Radiology. 1998 Feb; 26(3):297–303. [PubMed: 9587760]
29. Schrier RW, Wang W, Poole B, et al. Acute renal failure: definitions, diagnosis, pathogenesis, and therapy. J Clin Invest. 2004 Jul; 114(1):5–14. [PubMed: 15232604]
30. Wangsiripaisan A, Gengaro PE, Edelstein CL, et al. Role of polymeric Tamm-Horsfall protein in cast formation: oligosaccharide and tubular fluid ions. Kidney Int. 2001 Mar; 59(3):932–940. [PubMed: 11231348]
31. Jezzard P, Clare S. Sources of distortion in functional MRI data. Hum Brain Mapp. 1999; 8(2–3): 80–85. [PubMed: 10524596]

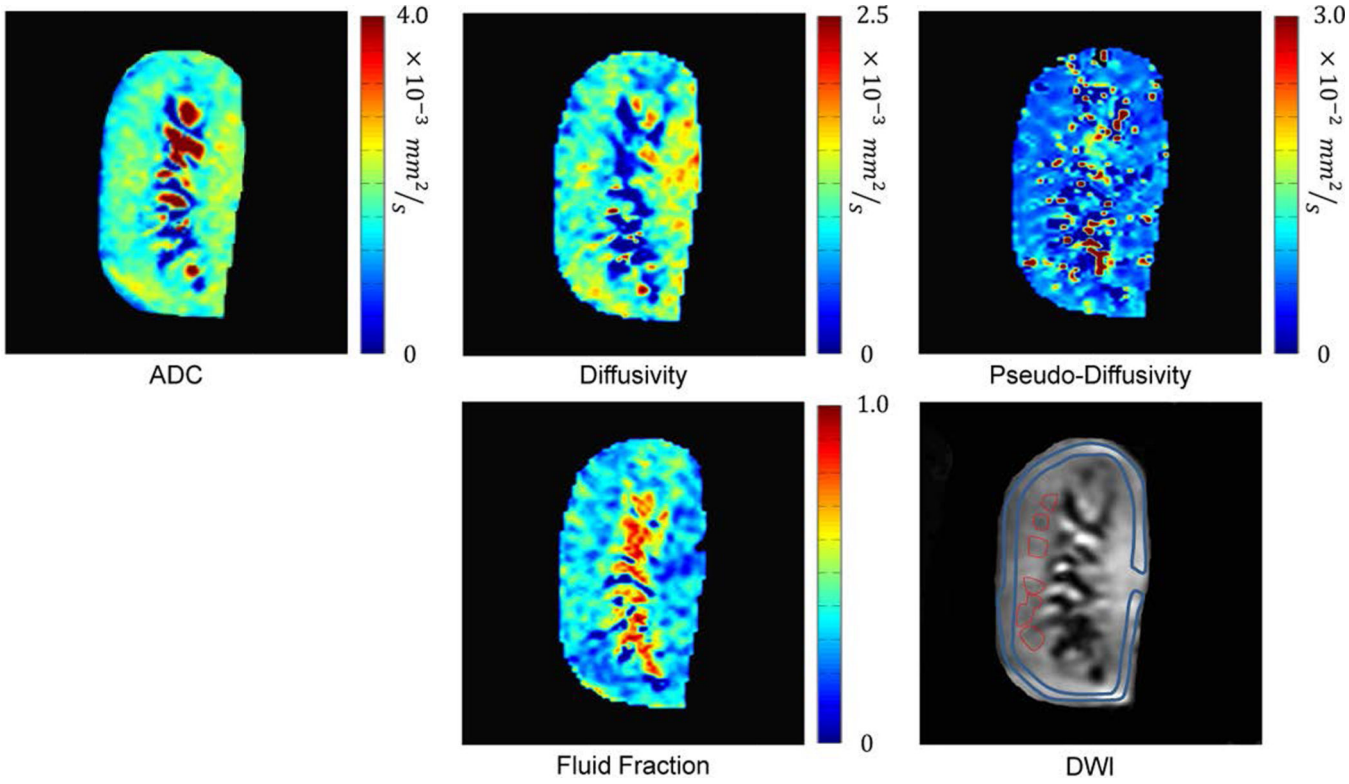

Figure 1.

DWI-derived ADC and IVIM maps. ADC, Diffusivity, pseudodiffusivity and fluid-fraction. Cortical (blue) and medullary (red) ROIs were drawn on b_0 DWI images and transferred to the maps.

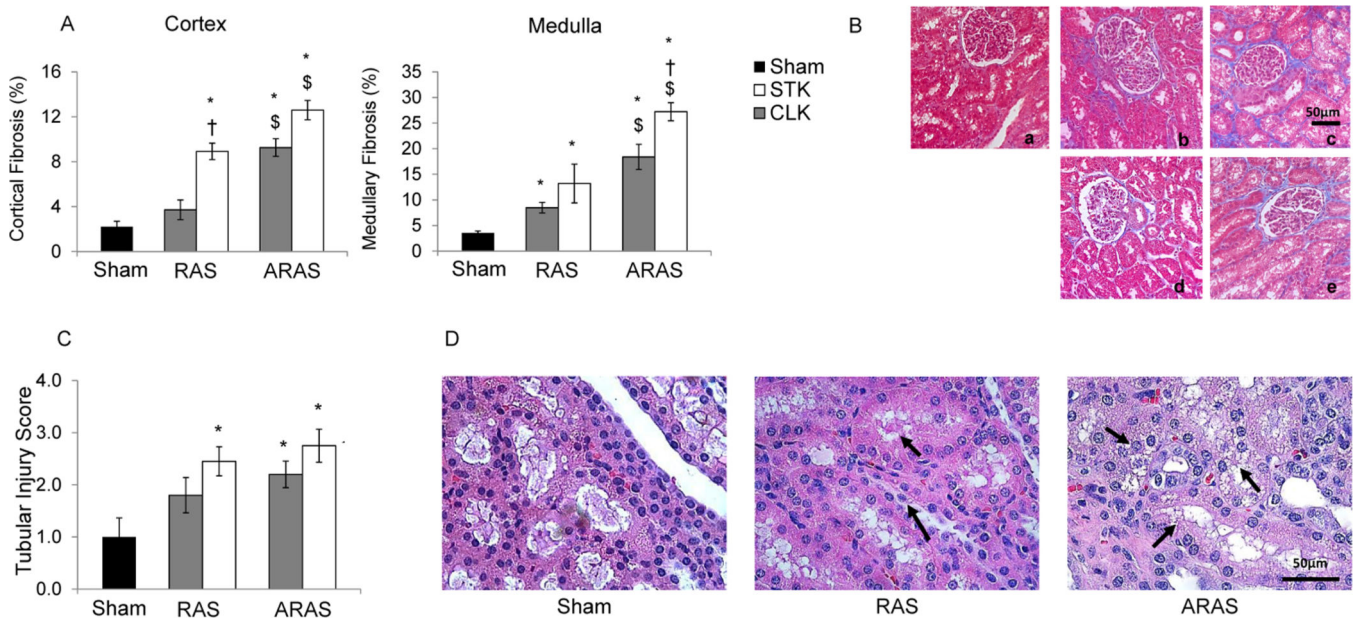

Figure 2.

Tissue Morphology. Cortical (left) and medullary (right) fibrosis were quantified from trichrome staining in Sham, contra-lateral (CLK) and stenotic (STK) kidneys in RAS and ARAS (A), as well as representative 20× images in Sham (a), STK and CLK of RAS (b,d) and ARAS (c,e), respectively (B). Semi-quantitative tubular injury scores (C) and hematoxylin-eosin images (40×) in Sham, RAS and ARAS (D) (*$p<0.05$ vs. Sham; †$p<0.05$ vs. CLK; \$$p<0.05$ RAS vs. ARAS). Cell detachment and cast formation are visible in RAS and ARAS tubules (arrows).

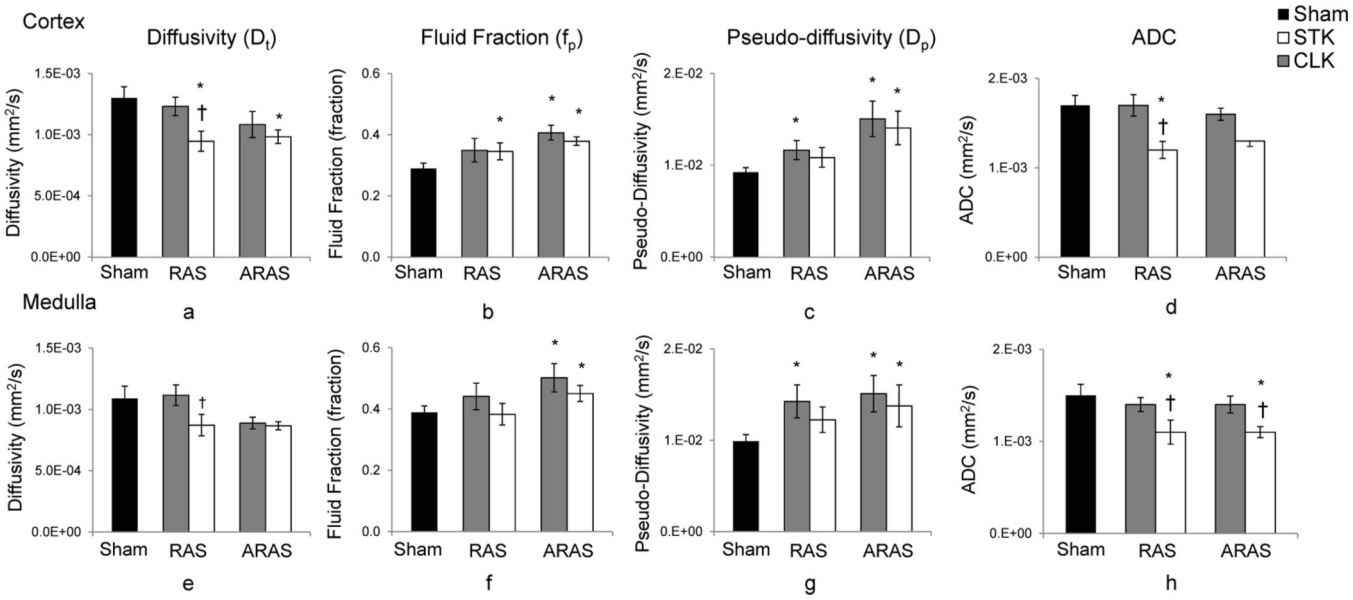

Figure 3.

DWI-derived ADC and IVIM parameters. In the cortex (a–d) and medulla (e–h) of Sham, stenotic (STK) and non-stenotic contra-lateral (CLK) kidneys of RAS and ARAS pigs. (*p<0.05 vs. Sham; †p<0.05 vs. CLK, correspondingly).

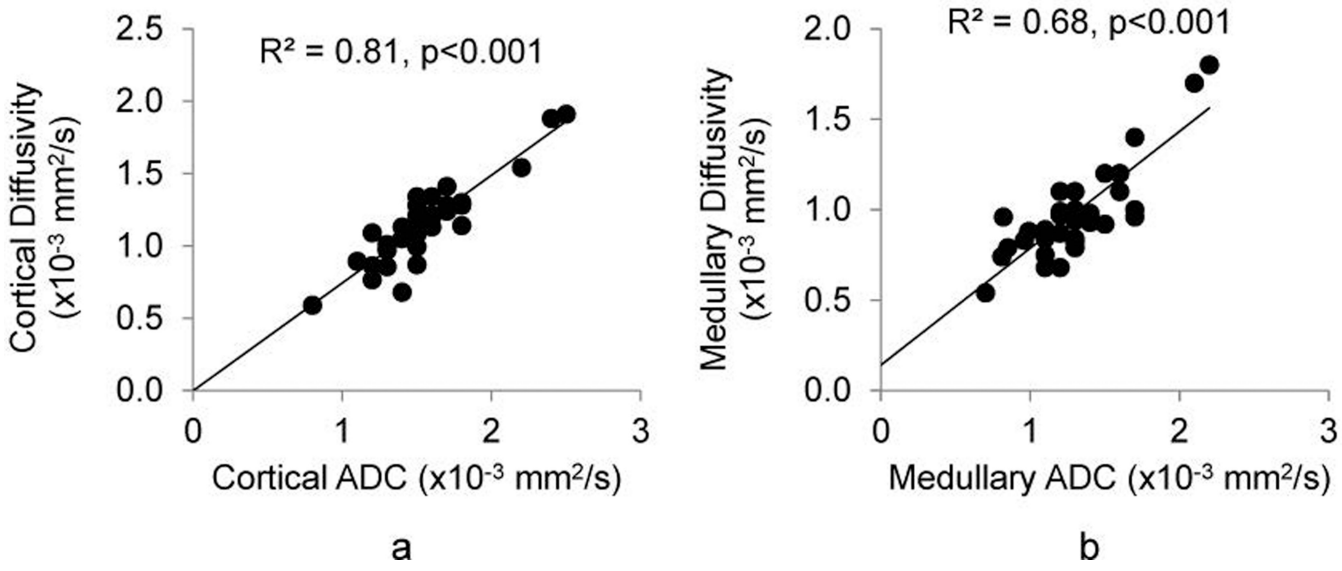

Figure 4.

ADC and diffusivity correlation. The two parameters demonstrated strong correlations in cortex (a) and medulla (b) of all kidneys.

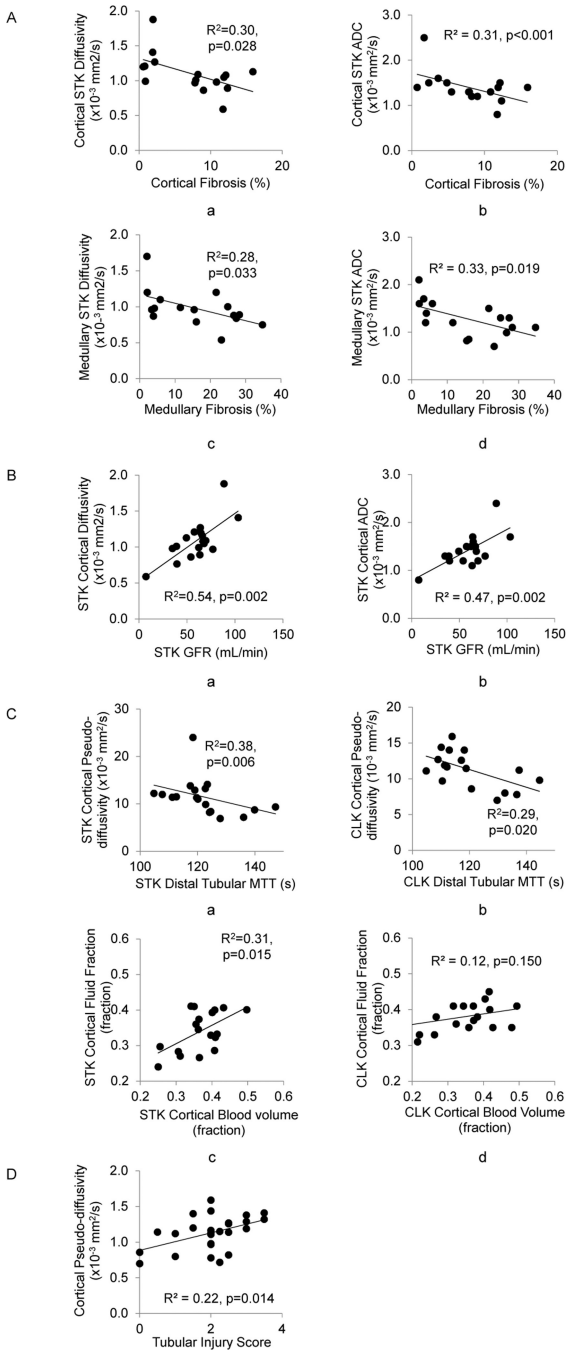

Figure 5.

Analyses of regression. Renal interstitial fibrosis (A). Cortical (a,b) and medullary (c,d) fibrosis levels correlated with diffusivity and ADC in corresponding compartments. The two markers also showed significant correlations with GFR (B). Furthermore, perfusion-dependent IVIM parameters showed correlation with renal functional parameters (C). Cortical pseudo-diffusivity correlated with distal tubular MTT in the stenotic kidney (STK) (a) and contra-lateral kidney (CLK) (b). Cortical fluid fraction in the STK showed a moderate but significant correlation with blood volume (c). These two parameters did not

correlate in CLK (d). A significant correlation was observed between the pseudo-diffusivity and tubular injury score (D).

Table 1

Renal hemodynamics and function in pigs after 16-weeks of Sham, RAS, and atherosclerotic RAS (ARAS).

Parameter	Sham (n=6)	RAS (n=7)		ARAS (n=6)	
Body weight (kg)	49±1	49±2		51±2	
Degree of Stenosis (%)	-	70±8*		77±4*	
MAP (mmHg)	98±3	119±7*		135±12*	
		STK	CLK	STK	CLK
Volume (cm^3)					
Cortex	94±3	67±12*†	125±10*	72±4*†	126±10*
Medulla	24±2	15±3*†	28±3	14±3*†	21±1
GFR (mL/min)	72±4	51±9*†	88±9*	53±6*†	92±6*
Regional GFR (mL/g/min)	0.76±0.04	0.75±.05	0.71±0.06	0.69±0.03	0.72±0.02
Total RBF (mL/min)	525±43	320±77*†	661±97	354±51*†	664±57
Cortical RBF	433±37	286±70*†	581±84	314±38*†	591±51
Medullary RBF	92±10	34±9*†	81±14	40±16*†	64±11
Perfusion (mL/g/min)					
Cortex	4.5±0.4	4.1±0.7	4.4±0.5	4.3±0.4	4.7±0.3
Medulla	3.9±0.7	2.2±0.3*	2.9±0.4	2.6±0.4	3.0±0.5
MTT (s)					
Cortical Vascular	7.9±0.6	9.2±1.1	8.4±0.8	8.9±0.2	8.5±0.4
Medullary vascular	76±3	77±2	73±2	73±1	68±5
Proximal tubular	42±2	42±2	45±3	42±1	41±0.5
Loop of Henle	74±3	77±4	73±2	73±1	68±5
Distal tubular	129±4	120±3	118±3	118±2*	112±1*†
FBV					
Cortical	0.35±0.02	0.35±0.03	0.38±0.01	0.38±0.01	0.40±0.01*
Medullary	0.43±0.04	0.32±0.03*	0.37±0.03	0.36±0.03*	0.37±0.03

MAP: Mean Arterial Pressure; RBF: Renal Blood Flow; FBV: Fractional Blood Volume, GFR: Glomerular Filtration Rate, MTT: Mean Transit Time

Stenotic Kidney (STK), Contra-lateral Kidney (CLK)

* $p<0.05$ vs. Sham;

† $p<0.05$ vs. CLK